Synthesis, structural characterization and chiroptical properties of lanarly and axially chiral boranils

Aurélie Macé, Khaoula Hamrouni, Paola Matozzo, Max Coehlo, Jakub Firlej, Faouzi Aloui, Nicolas Vanthuyne, Elsa Caytan, Marie Cordier, Grégory Pieters, et al.

Synthesis, Structural Characterization and Chiroptical Properties of Planarly and Axially Chiral Boranils

Aurélie Macé,[a] Khaoula Hamrouni,[a,b] Paola Matozzo,[a] Max Coehlo,[c] Jakub Firlej,[d] Faouzi Aloui,[b] Nicolas Vanthuyne,[e] Elsa Caytan,[a] Marie Cordier,[a] Grégory Pieters,[c] Monika Srebro-Hooper,*[d] Fabienne Berrée,*[a] Bertrand Carboni,[a] Jeanne Crassous*[a]

Abstract: 2-Amino[2.2]paracyclophane reacts with salicylaldehyde or 2-hydroxyacetophenone to yield imines that then give access to a new series of boranils (**8b**-**d**) upon complexation with BF_2. These novel boron-containing compounds display both planar and axial chiralities, and were examined experimentally and computationally. In particular, their photophysical and chiroptical properties were studied and compared to newly prepared, more simple boranils (**9a**-**d**) exhibiting axial chirality only. Simpler chiral architectures were shown to demonstrate overall stronger CPL activity.

Keywords: boranil • axial chirality • planar chirality • optical activity • density functional calculations

Introduction

Circularly polarized luminescence (CPL), a phenomenon that reflects the difference of emission of right and left circularly polarized light by an enantiomerically pure compound, is the source of promising applications in 3D displays, data storage, tunable lasers, biosensors, etc.[1] The search for novel simple organic molecules that may act as chiral emitters, in complement to organometallic complexes, is therefore of prime importance to enable further developments in these fields. In recent years, boron-containing compounds, which stimulated more and more interest due to their substantial impact in organic synthesis and catalysis, have also found innovative applications in the areas of organic light-emitting diodes (OLEDs), biosensing and bioimaging.[2] While boron dipyrromethene (BODIPY) scaffolds remain among the most popular class of boronated organic dyes since their discovery in the late 1960s,[3,4] numerous other organoboranes possessing a triaryl moiety or a four-coordinate boron(III) atom, for example, have also found outstanding applications as functional materials.[5] Among them, boranils that are based on a salicylaldimine core have shown to be promising options, especially due to their easy access and high chemical stability.[6]

To our knowledge, few examples of CPL-active boranils have been hitherto reported (Figure 1). J.-J. Kim, J. Yoon *et al.* synthesized a binuclear boron complex **1** with (*1R,2R*)-1,2-cyclohexanediamine as linker to fix two pyrene rings.[7] S. Guieu *et al.* described the synthesis and the aggregation-induced emission enhancement of boranils **2** based on (*S*)- and (*R*)-α-methylbenzylamine.[8] Axially chiral boron difluoride complexes **3a**-**b**, derived from an (*R*)-/(*S*)-1,1′-binaphthol unit, were reported by X. Wang, Z. Liu *et al*.[9] More recently, our groups studied both experimentally and theoretically the chiroptical properties of chiral emissive helicene-boranils **4** and **5**, and highlighted the combined helical and axial chirality effects.[10] Lastly, while this work was in progress, organoboranes **6a**-**6i** and **7** combining one or two BF_2 moieties directly with the benzene rings of an (R_p)-/(S_p)- [2.2]paracyclophane (PCP) unit have been designed and their aggregation-amplified CPL emission have been studied, demonstrating fluorescence dissymmetry factors $|g_{lum}|$ up to 7.6×10^{-3} in THF/water solution.[11]

Although such systems may appear as potential candidates for CPL applications, they often require multistep synthesis that makes structural variations difficult and time-consuming, which strongly influences the cost of the final material. In order to provide a solution to these drawbacks and in continuation to our previous works on boron-substituted helicene derivatives,[10] we pursue the exploration of the chiroptical properties of new chiral organoborane systems. Herein, we report the synthesis, structural characterization, HPLC resolution, and examination of photophysical and chiroptical properties of new boranils **8** and **9** with planar and / or axial chirality (Figure 2). To shed light on their stereochemical and spectroscopic features, their

[a] *Dr. A. Macé, P. Matozzo, Dr. E. Caytan, Dr. M. Cordier, Dr. F. Berrée, Dr. B. Carboni, Dr. J. Crassous*
Univ Rennes, CNRS, ISCR-UMR 6226, ScanMAT-UMS 2001, F-35000 Rennes, France.
E-mails: fabienne.berree@univ-rennes1.fr, jeanne.crassous@univ-rennes1.fr

[b] *K. Hamrouni, Dr. F. Aloui*
University of Monastir, Laboratory of Asymmetric Synthesis and Molecular Engineering of Organic Materials for Organic Electronics (LR18ES19), Faculty of Sciences, Avenue of Environment, Monastir 5019,Tunisia.

[c] *M. Coehlo, Dr. G. Pieters*
Université Paris-Saclay, CEA, Département Médicaments et Technologies pour la Santé (DMTS), SCBM, Gif-sur-Yvette, F-91191, France.

[d] *J. Firlej, Prof. M. Srebro-Hooper*
Faculty of Chemistry, Jagiellonian University, Gronostajowa 2, 30-387 Krakow, Poland.
E-mail: srebro@chemia.uj.edu.pl

[e] *Dr. N. Vanthuyne*
Aix Marseille University, CNRS, Centrale Marseille, iSm2, Marseille, France.

Received: ((will be filled in by the editorial staff))
Revised: ((will be filled in by the editorial staff))
Published online: ((will be filled in by the editorial staff))

experimental analyses have been complemented by quantum-chemical calculations.

Materials and Methods

General Experimental Details. Solvents were freshly distilled under argon from sodium / benzophenone (toluene) or from phosphorus pentoxide (1,2-DCE = 1,2-dichloroethane). Column chromatography purifications were performed over silica gel (Merck Geduran 60, 0.063-0.200 mm). Flash chromatography purifications were carried out on a Grace RevelerisTM with PuriflashTM 40µm flash cartridges (Buchi). ^{1}H, ^{13}C, ^{19}F and ^{11}B NMR spectra were recorded at room temperature on Bruker AV III spectrometers, from 300 to 500 MHz, using deuterated chloroform as solvent. The terms s, d, t, q, m indicate respectively singlet, doublet, triplet, quartet, multiplet; br stands for broad; dd is doublet of doublets, dt - doublet of triplets, td - triplet of doublets. Mass spectrometry was performed by the CRMPO, University of Rennes 1, on an LC-MS Agilent 6510, a Brucker MaXis 4G or a Thermo Fisher Q-Exactive using ESI and ASAP techniques. Melting points were measured on a melting point apparatus Stuart SMP10. Specific rotations (in deg $cm^3g^{-1}dm^{-1}$) were measured on a Jasco P-2000 polarimeter with a sodium lamp (589 nm) in a 10 cm cell, thermostated at 25 °C with a Peltier controlled cell holder. Circular dichroism (in $M^{-1}cm^{-1}$) was recorded on a Jasco J-815 Circular Dichroism Spectrometer IFR140 facility (Biosit platform - Université de Rennes 1). UV-vis spectroscopy was conducted on a Varian Cary 5000 spectrometer. Chiral high-performance liquid chromatography (HPLC) was performed by iSm2, Aix Marseille University, on an Agilent Technologies 1260 Infinity with Igloo-Cil ovens, using Jasco P-2000 and CD-2095 as polarimetric and circular dichroism detectors, respectively. The analytical (250×4.6 mm) and preparative (250×10 mm) columns used were (*S*,*S*)-Whelk-O1 from Regis Technologies (Morton Grove, USA) and Chiralpak IC, ID, and IH. Beforehand circularly polarized luminescence (CPL) measurements, absorption spectra were recorded on an UV-CARY 50 and optical density was checked to be below 0.1 for the first absorption transition. Then, emission spectra were recorded with Fluoromax-3 (Horiba) spectrofluorometer. The subsequent CPL measurements were performed using a commercialized instrument JASCO CPL-300 at room temperature in a 10×10 mm cell.

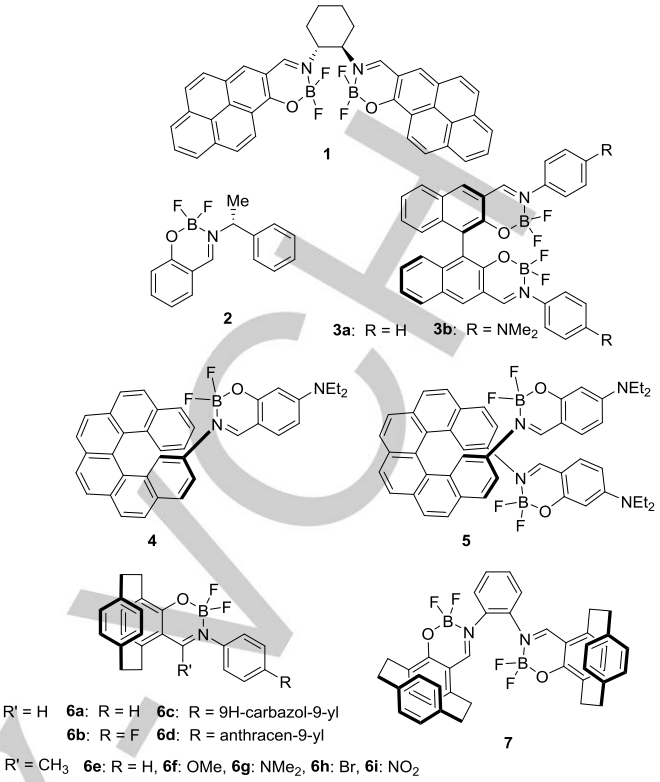

FIGURE 1. Chemical structures of selected known CPL-active chiral boranils (for clarity, a single enantiomer is presented in each case).

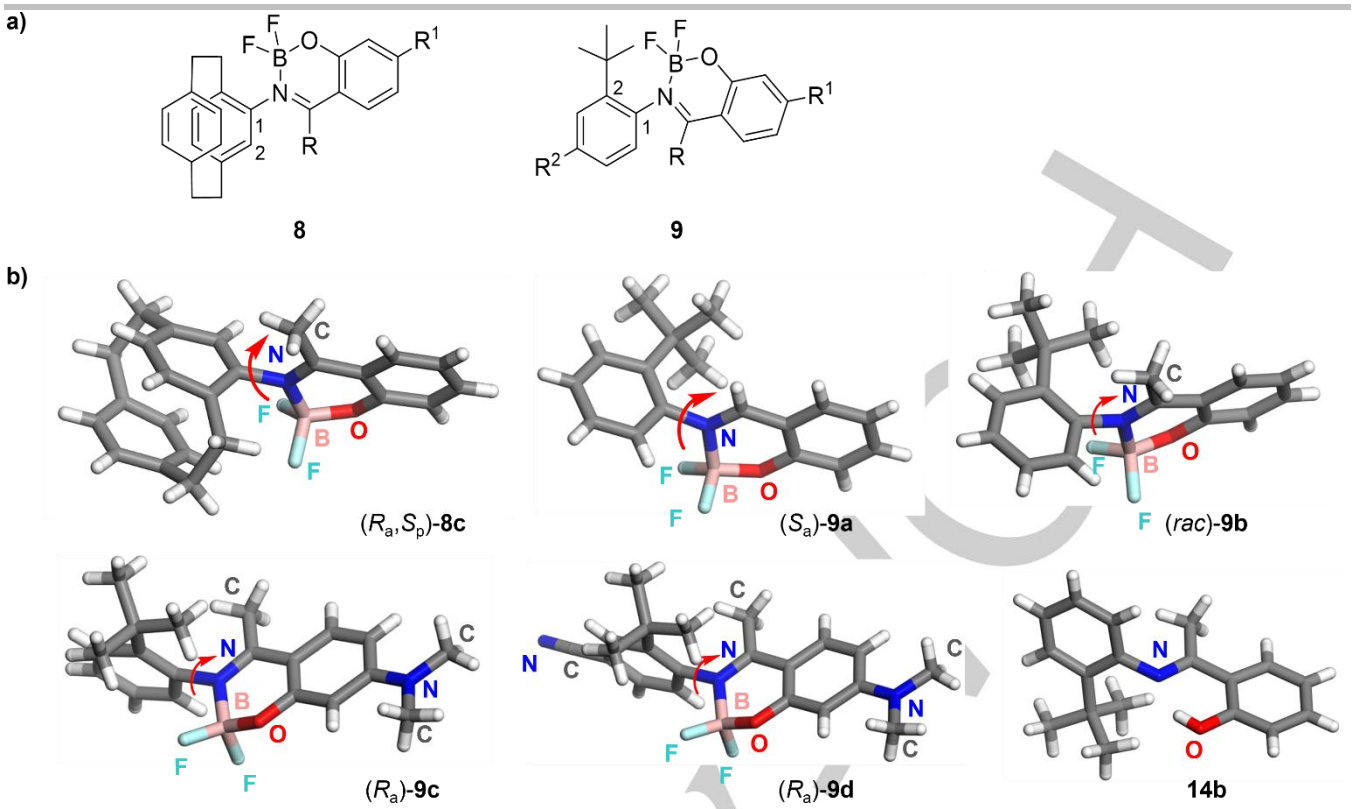

FIGURE 2. a) Chemical structures of novel planarly and / or axially chiral boranils **8** and **9** studied in this work. For a definition of R, R^1 and R^2, see Schemes 1 and 2. b) X-ray diffraction structures of (R_a,S_p)-**8c** ((+)-**8c**, first eluted enantiomer, see SI), (S_a)-**9a**, (*rac*)-**9b** (only the S_a enantiomer shown), (R_a)-**9c** and (R_a)-**9d** displaying axial chirality, and of precursor **14b**.

General procedure for the synthesis of imines 12 and 14 (except 14a). Titanium ethoxide (228 mg, 0.2 mL, 1 mmol) was added to a solution of 4-amino[2.2]paracyclophane **10** or aniline derivative **13** (0.5 mmol) and compound **11** (0.5 mmol) in dry toluene (5 mL). This mixture was heated at 100 °C for one night and then an additional equivalent of titanium ethoxide (0.1 mL, 0.5 mmol) was added. The solution was stirred at 100 °C for another 4 hours. The resultant solution was quenched by addition of water (1 mL). After extraction with dichloromethane, and subsequent filtration through a pad of celite, the organic phase was dried over $MgSO_4$ and concentrated under reduced pressure. The resulting solid was washed with cold methanol or cold diisopropylether or was purified by chromatography (silica gel, cyclohexane / EtOAc as eluent) to afford the imine **12** or **14**.

(E)-2-((1,4(1,4)-dibenzenacyclohexaphane-12-ylimino)methyl)phenol (12a). Obtained as a yellow solid (116 mg, 71%) after a chromatography over silica gel (cyclohexane/EtOAc: 100/0 to 95/5). Mp = 124-126 °C. R_f = 0.72 (cyclohexane/EtOAc: 8/2). ^{1}H NMR (300 MHz, $CDCl_3$) δ 13.93 (s, 1H), 8.37 (s, 1H), 7.54-7.39 (m, 2H), 7.18 (d, *J* = 8.2 Hz, 1H), 7.03 (t, *J* = 7.4 Hz, 1H), 6.91 (dd, *J* = 7.9, 1.9 Hz, 1H), 6.70-6.54 (m, 4H), 6.43 (d, *J* = 7.9 Hz, 1H), 6.07 (s, 1H), 3.80-3.61 (m, 1H), 3.29 (dd, *J* = 9.6, 5.1 Hz, 2H), 3.22-3.03 (m, 4H), 2.88 (dt, *J* = 12.9, 8.7 Hz, 1H). ^{13}C{^{1}H} NMR (75 MHz, $CDCl_3$) δ 161.2, 161.0, 146.7, 142.0, 139.9, 139.1, 135.0, 134.8, 133.5, 133.12, 133.06, 132.1, 131.9, 131.8, 129.2, 125.4, 119.7, 119.2, 117.3, 35.4, 35.0, 34.3, 32.7. HRMS (ESI$^+$) *m/z* [M+H]$^+$ calcd for $C_{23}H_{22}NO$ 328.1701, found 328.1702.

(E)-2-((1,4(1,4)-dibenzenacyclohexaphane-12-ylimino)methyl)-5-(dimethylamino)phenol (12b). Obtained as a yellow solid (144 mg, 78%) after a chromatography over silica gel (cyclohexane/EtOAc: 9/1 to 8/2). Mp = 98-100 °C. R_f = 0.35 (cyclohexane/EtOAc: 8/2). ^{1}H NMR (300 MHz, $CDCl_3$) δ 14.54 (s, 1H), 8.15 (s, 1H), 7.18 (d, *J* = 8.4 Hz, 1H), 6.85 (dd, *J* = 7.9, 2.0 Hz, 1H), 6.62-6.41 (m, 4H), 6.40-6.23 (m, 3H), 5.98 (s, 1H), 3.62 (ddd, *J* = 13.0, 8.5, 3.4 Hz, 1H), 3.27-2.92 (m, 12H), 2.86-2.69 (m, 1H). ^{13}C{^{1}H} NMR (75 MHz, $CDCl_3$) δ 164.6, 158.9, 154.2, 146.7, 141.7, 140.0, 139.0, 134.9, 133.9, 133.5, 133.4, 133.0, 131.8, 130.3, 129.0, 125.0, 110.1, 104.2, 98.7, 40.2, 35.4, 35.1, 34.2, 32.8. HRMS (ESI$^+$) *m/z* [M+H]$^+$ calcd for $C_{25}H_{27}N_2O$ 371.2123, found 371.2124.

(E)-2-(1-(1,4(1,4)-dibenzenacyclohexaphane-12-ylimino)ethyl)phenol (12c). Obtained as a yellow solid (113 mg, 66%) after a chromatography over silica gel (cyclohexane/EtOAc: 95/5 to 9/1). Mp = 176-178 °C. R_f = 0.92 (cyclohexane/EtOAc: 8/2). ^{1}H NMR (400 MHz, $CDCl_3$) δ 15.70 (s, 1H), 7.64 (dd, *J* = 7.9, 1.8 Hz, 1H), 7.53-7.34 (m, 1H), 7.15 (dd, *J* = 8.1, 1.7 Hz, 2H), 7.04-6.85 (m, 1H), 6.65 (dd, *J* = 7.8, 2.1 Hz, 1H), 6.61-6.46 (m, 4H), 5.80 (d, *J* = 1.7 Hz, 1H), 3.34-3.21 (m, 2H), 3.21-3.09 (m, 4H), 3.00 (ddd, *J* = 12.6, 7.3, 4.6 Hz, 1H), 2.80-2.72 (m, 1H), 2.22 (s, 3H). ^{13}C{^{1}H} NMR (101 MHz, $CDCl_3$) δ 170.0, 162.5, 144.5, 141.0, 139.8, 139.2, 135.1, 133.5, 133.1, 133.0, 132.4, 132.2, 130.1, 129.2, 128.9, 127.8, 120.0, 118.3, 118.2, 35.5, 35.1, 34.3, 32.4, 17.4. HRMS (ESI$^+$) *m/z* [M+H]$^+$ calcd for $C_{24}H_{24}NO$ 342.1858, found 342.1851.

(E)-2-(1-(1,4(1,4)-dibenzenacyclohexaphane-12-ylimino)ethyl)-5-(dimethylamino)phenol (12d). Obtained as a brown solid (136 mg, 71%) by washing with cold methanol. Mp = 153-154 °C. ^{1}H NMR (300 MHz, $CDCl_3$) δ 16.41 (s, 1H), 7.45 (d, *J* = 8.9 Hz, 1H), 7.17 (d, *J* = 7.9 Hz, 1H), 6.62 (d, *J* = 7.9 Hz, 1H),

6.56-6.47 (m, 4H), 6.34 (d, *J* = 2.7 Hz, 1H), 6.29 (d, *J* = 9.0 Hz, 1H), 5.81 (s, 1H), 3.31-3.22 (m, 2H), 3.08 (s, 6H), 3.10-2.97 (m, 5H), 2.75-2.68 (m, 1H), 2.13 (s, 3H). $^{13}C\{^1H\}$ NMR (75 MHz, $CDCl_3$) *δ* 165.2, 158.5, 152.0, 146.6, 141.7, 140.0, 138.9, 134.9, 133.8, 133.6, 133.5, 133.0, 131.8, 130.1, 129.0, 124.9, 109.7, 103.9, 98.0, 44.7, 35.4, 35.1, 34.2, 32.8, 12.8. HRMS (ESI^+) *m/z* $[M+H]^+$ calcd for $C_{26}H_{29}N_2O$ 385.2280, found 385.2279.

(E)-2-(((2-(tert-butyl)phenyl)imino)methyl)phenol (14a).[12] A solution of 2-*tert*-butylaniline (745 mg, 5 mmol) and 2-hydroxybenzaldehyde (610 mg, 5 mmol) in ethanol (7 mL) was refluxed overnight. The resultant mixture was concentrated under vacuum to give a yellow solid (923 mg, 73%) which was washed with cold diisopropylether. Mp = 99-100 °C. ^1H NMR (300 MHz, $CDCl_3$) *δ* 13.02 (brs, 1H), 8.44 (s, 1H), 7.47-7.40 (m, 3H), 7.31-7.24 (m, 2H), 7.11-7.02 (m, 1H), 6.97 (td, *J* = 7.4, 1.1 Hz, 1H), 6.90 (dd, *J* = 7.0, 2.2 Hz, 1H), 1.44 (s, 9H). $^{13}C\{^1H\}$ NMR (75 MHz, $CDCl_3$) *δ* 162.8, 160.7, 149.2, 142.9, 133.3, 132.5, 127.4, 126.6, 126.4, 121.1, 119.5, 119.2, 117.2, 35.3, 30.9.

(E)-2-(1-((2-(tert-butyl)phenyl)imino)ethyl)phenol (14b). Obtained as a yellow solid (85 mg, 64%) by washing with cold diisopropylether. Mp = 120-122 °C. ^1H NMR (300 MHz, $CDCl_3$) *δ* 14.85 (brs, 1H), 7.68 (dd, *J* = 8.0, 1.6 Hz, 1H), 7.51 (dd, *J* = 7.6, 1.8 Hz, 1H), 7.43 (ddd, *J* = 8.5, 7.2, 1.7 Hz, 1H), 7.33-7.15 (m, 2H), 7.09 (d, *J* = 8.3 Hz, 1H), 6.95 (t, *J* = 7.6 Hz, 1H), 6.65 (dd, *J* = 7.4, 1.8 Hz, 1H), 2.33 (s, 3H), 1.39 (s, 9H). $^{13}C\{^1H\}$ NMR (75 MHz, $CDCl_3$) *δ* 170.8, 162.2, 146.1, 141.1, 133.2, 129.0, 126.9, 126.7, 125.1, 122.6, 119.9, 118.4, 118.3, 35.2, 30.4, 18.2. HRMS (ESI^+) *m/z* $[M+Na]^+$ calcd for $C_{18}H_{21}NNaO$ 290.1521, found 290.1516.

(E)-2-(1-((2-(tert-butyl)phenyl)imino)ethyl)-5-(dimethylamino)phenol (14c). Obtained as a brown solid (78 mg, 50%) by washing with cold diisopropylether. Mp = 134-135 °C. ^1H NMR (300 MHz, $CDCl_3$) *δ* 15.32 (brs, 1H), 7.54-7.43 (m, 2H), 7.20 (td, *J* = 7.4, 1.7 Hz, 1H), 7.13 (td, *J* = 7.5, 1.7 Hz, 1H), 6.64 (dd, *J* = 7.5, 1.7 Hz, 1H), 6.32-6.24 (m, 2H), 3.05 (s, 6H), 2.22 (s, 3H), 1.36 (s, 9H). $^{13}C\{^1H\}$ NMR (75 MHz, $CDCl_3$) *δ* 169.3, 164.2, 153.9, 146.3, 141.5, 130.1, 126.6, 126.5, 124.5, 123.5, 109.9, 103.2, 99.3, 40.0, 35.1, 30.4, 17.5. HRMS (ESI^+) *m/z* $[M+Na]^+$ calcd for $C_{20}H_{26}N_2NaO$ 333.1943, found 333.1942.

3-(tert-butyl)-4-((1-(2-hydroxyphenyl)ethylidene)amino)benzonitrile (14d). Obtained as a yellow solid (100 mg, 60%) after a chromatography over silica gel (cyclohexane/EtOAc: 9/1 to 8/2). Mp = 211-213 °C. R_f = 0.37 (cyclohexane/EtOAc: 8/2). ^1H NMR (300 MHz, $CDCl_3$) *δ* 14.20 (s, 1H), 7.70 (d, *J* = 1.8 Hz, 1H), 7.47 (d, *J* = 8.0 Hz, 1H), 7.46 (d, *J* = 8.9 Hz, 1H), 6.68 (d, *J* = 8.0 Hz, 1H), 6.27 (dd, *J* = 8.9, 2.6 Hz, 1H), 6.23 (d, *J* = 2.6 Hz, 1H), 3.04 (s, 6H), 2.18 (s, 3H), 1.33 (s, 9H). $^{13}C\{^1H\}$ NMR (75 MHz, $CDCl_3$) *δ* 169.5, 163.5, 154.3, 151.4, 142.9, 131.2, 130.5, 124.1, 119.8, 109.4, 107.6, 103.7, 99.0, 40.1, 35.5, 30.0, 18.2. HRMS (ESI^+) *m/z* $[M+Na]^+$ calcd for $C_{21}H_{25}N_3NaO$ 358.1890, found 358.1893.

General procedure for the synthesis of boranils 8 and 9. To a solution of the imine **12** or **14** (1.0 eq.) in dry 1,2-DCE (7 mL/mmol) at 60 °C, under an inert argon atmosphere, were added boron trifluoride ethyl etherate (2.0 eq.) and *N*,*N*-diisopropylethylamine (DIEA) (2.0 eq.). The solution was stirred at 85 °C for 7 hours and then additional 2.0 equivalents of boron trifluoride ethyl etherate and DIEA were added. The solution was stirred at 85 °C for another 21 hours. The solvent was removed under vacuum and the resulting crude material was diluted with methylene chloride and washed with a sodium bicarbonate saturated aqueous solution. The organic layer was then dried over $MgSO_4$ and concentrated under reduced pressure. The residue was subjected to chromatography (silica gel, cyclohexane/CH_2Cl_2 as eluent) to afford the boranil derivative **8** or **9**.

3-(1,4(1,4)-dibenzenacyclohexaphane-1^2-yl)-2,2-difluoro-N,N-dimethyl-4a,5-dihydro-2H-2λ^4,3λ^4-benzo[e][1,3,2]oxazaborinin-7-amine (8b). Obtained from 104 mg of **12b** as a yellow solid (108 mg, 92%) after a chromatography over silica gel (cyclohexane/CH_2Cl_2: 5/5 to 3/7). Mp = 280-282 °C (dec.). R_f = 0.15 (cyclohexane/CH_2Cl_2: 4/6). ^1H NMR (300 MHz, $CDCl_3$) *δ* 7.74 (brs, 1H), 7.21 (d, *J* = 8.9 Hz, 1H), 6.95 (d, *J* = 1.6 Hz, 1H), 6.80 (dd, *J* = 7.9, 1.9 Hz, 1H), 6.68 (dd, *J* = 7.9, 1.9 Hz, 1H), 6.62 (dd, *J* = 7.8, 1.9 Hz, 1H), 6.60 (dd, *J* = 8.1, 1.9 Hz, 1H), 6.51 (d, *J* = 7.8 Hz, 1H), 6.42-6.35 (m, 2H), 6.31 (d, *J* = 2.2 Hz, 1H), 3.25-2.99 (m, 7H), 3.14 (s, 6H), 2.93-2.80 (m, 1H). $^{13}C\{^1H\}$ NMR (75 MHz, $CDCl_3$) *δ* 163.0, 162.2, 158.6, 144.0, 141.6, 139.6, 139.4, 137.4, 134.7, 134.2, 133.8, 132.9, 132.5, 132.1, 127.4, 108.0, 107.2, 99.4, 40.8, 36.1, 35.8, 35.4, 32.4. $^{11}B\{^1H\}$ NMR (96 MHz, $CDCl_3$) *δ* 1.1 (dd, *J* = 21.9, 13.5 Hz). $^{19}F\{^1H\}$ NMR (282 MHz, $CDCl_3$) *δ* -133.3 (dq, *J* = 84.1, 21.9 Hz), -141.6 (dq, *J* = 84.1, 13.5 Hz). HRMS (ESI^+) *m/z* $[M+Na]^+$ calcd for $C_{25}H_{25}{}^{11}B^{19}F_2N_2NaO$ 441.1926, found 441.1925.

3-(1,4(1,4)-dibenzenacyclohexaphane-1^2-yl)-2,2-difluoro-4-methyl-2H-2λ^4,3λ^4-benzo[e][1,3,2]oxazaborinine (8c). Obtained from 87 mg of **12c** as a beige solid (70 mg, 71%) after a chromatography over silica gel (cyclohexane/CH_2Cl_2: 6/4 to 4/6). Mp = 238-240 °C (dec.). R_f = 0.4 (cyclohexane/CH_2Cl_2: 4/6). ^1H NMR (300 MHz, $CDCl_3$) *δ* 7.66-7.55 (m, 2H), 7.22 (dd, *J* = 8.5, 1.2 Hz, 1H), 7.10 (d, *J* = 7.9 Hz, 1H), 7.00 (ddd, *J* = 8.5, 7.3, 1.2 Hz, 1H), 6.74-6.67 (m, 3H), 6.58 (d, *J* = 7.9 Hz, 1H), 6.44 (d, *J* = 1.0 Hz, 2H), 3.40-3.18 (m, 3H), 3.07-2.84 (m, 5H), 2.13 (s, 3H). $^{13}C\{^1H\}$ NMR (75 MHz, $CDCl_3$) *δ* 175.2 (d, *J* = 1.9 Hz), 158.9 (d, *J* = 4.6 Hz), 140.9, 139.2, 139.0, 138.4, 137.7, 135.5, 134.7, 134.4, 133.4 (d, *J* = 1.9 Hz), 133.3 (d, *J* = 1.9 Hz), 132.1, 131.5, 129.4, 127.0 (d, *J* = 4.3 Hz), 120.5, 120.2, 35.24, 35.21, 35.0, 30.5, 18.8. $^{11}B\{^1H\}$ NMR (96 MHz, $CDCl_3$) *δ* 0.65 (dd, *J* = 22.0, 9.0 Hz). $^{19}F\{^1H\}$ NMR (282 MHz, $CDCl_3$) *δ* -134.0 (dq, *J* = 79.6, 22.0 Hz), -142.2 (dq, *J* = 79.6, 9.0 Hz). HRMS (ESI^+) *m/z* $[M+Na]^+$ calcd for $C_{24}H_{22}NO^{19}F_2{}^{11}BNa$ 412.1655, found 412.1658.

3-(1,4(1,4)-dibenzenacyclohexaphane-1^2-yl)-2,2-difluoro-N,N,4-dimethyl-2H-2λ^4,3λ^4-benzo[e][1,3,2]oxazaborinin-7-amine (8d). Obtained from 127 mg of **12d** as a yellow solid (65 mg, 46%) after a chromatography over silica gel (cyclohexane/CH_2Cl_2: 6/4 to 4/6). Mp = 246-248 °C (dec.). R_f = 0.3 (cyclohexane/CH_2Cl_2: 4/6). ^1H NMR (300 MHz, $CDCl_3$) *δ* 7.40 (d, *J* = 8.7 Hz, 1H), 7.10 (d, *J* = 8.1 Hz, 1H), 6.77-6.64 (m, 3H), 6.58 (d, *J* = 7.9 Hz, 1H), 6.44-6.29 (m, 4H), 3.42-3.13 (m, 3H), 3.10 (s, 6H), 3.04-2.80 (m, 5H), 1.99 (s, 3H). $^{13}C\{^1H\}$ NMR (75 MHz, $CDCl_3$) *δ* 171.3, 160.8, 157.0, 140.4, 139.3, 138.9, 136.0, 135.2, 134.5, 134.0, 133.6, 133.5, 132.0, 131.4, 131.1, 127.8, 107.9, 106.1, 99.5, 40.2, 35.3, 35.2, 35.0, 30.7, 18.0. $^{11}B\{^1H\}$ NMR (96 MHz, $CDCl_3$) *δ* 0.7 (dd, *J* = 21.6, 13.5 Hz). $^{19}F\{^1H\}$ NMR (282 MHz, $CDCl_3$) *δ* -135.9 (dq, *J* = 83.4, 21.2 Hz),

- 141.6 (dq, *J* = 83.4, 12.9 Hz). HRMS (ESI$^+$) *m/z* [M+Na]$^+$ calcd for $C_{26}H_{27}{}^{11}B^{19}F_2N_2NaO$ 455.2082, found 455.2076.

3-(2-(tert-butyl)phenyl)-2,2-difluoro-2H-2λ^4,3λ^4-benzo[e][1,3,2]oxazaborinine (9a). Obtained from 605 mg of **14a** as a yellow solid (374 mg, 52%) after a chromatography over silica gel (cyclohexane/CH_2Cl_2: 6/4 to 4/6). Mp = 163-164 °C. R_f = 0.54 (cyclohexane/CH_2Cl_2: 6/4). ^{1}H NMR (300 MHz, $CDCl_3$) *δ* 8.32 (brs, 1H), 7.70 (ddd, *J* = 8.7, 7.2, 1.7 Hz, 1H), 7.63 (dd, *J* = 8.1, 1.4 Hz, 1H), 7.48 (dd, *J* = 7.8, 1.7 Hz, 1H), 7.44-7.27 (m, 3H), 7.22 (d, *J* = 8.1 Hz, 1H), 7.07 (td, *J* = 7.5, 1.0 Hz, 1H), 1.37 (s, 9H). ^{13}C{^{1}H} NMR (75 MHz, $CDCl_3$) *δ* 166.9, 160.3 (d, *J* = 4.9 Hz), 144.1, 140.2, 139.3 (d, *J* = 6.3 Hz), 132.2 (d, *J* = 7.2 Hz), 129.8 (d, *J* = 4.3 Hz), 129.1, 127.8, 126.9, 120.6 (d, *J* = 6.3 Hz), 120.1, 115.5, 36.6, 33.2. ^{11}B{^{1}H} NMR (96 MHz, $CDCl_3$) *δ* 0.9 (d, *J* = 25.3 Hz). ^{19}F{^{1}H} NMR (282 MHz, $CDCl_3$) *δ* -130.2 (dq, *J* = 76.9, 24.6 Hz), -146.5 (d, *J* = 83.4 Hz). HRMS (ESI$^+$) *m/z* [M+Na]$^+$ calcd for $C_{17}H_{18}{}^{11}B^{19}F_2NNaO$ 324.1347, found 324.1341.

3-(2-(tert-butyl)phenyl)-2,2-difluoro-4-methyl-2H-2λ^4,3λ^4-benzo[e][1,3,2]oxazaborinine (9b). Obtained from 150 mg of **14b** as a yellow solid (97 mg, 55%) after a chromatography over silica gel (cyclohexane/CH_2Cl_2: 6/4 to 4/6). Mp = 171-172 °C. R_f = 0.52 (cyclohexane/CH_2Cl_2: 5/5). ^{1}H NMR (300 MHz, $CDCl_3$) *δ* 7.69 (dd, *J* = 8.1, 1.6 Hz, 1H), 7.66-7.60 (m, 2H), 7.40 (td, *J* = 7.7, 1.6 Hz, 1H), 7.29 (td, *J* = 7.5, 1.5 Hz, 1H), 7.20 (dd, *J* = 8.4, 1.2 Hz, 1H), 7.11 (dt, *J* = 7.9, 1.9 Hz, 1H), 7.05 (td, *J* = 7.5, 1.2 Hz, 1H), 2.42 (s, 3H), 1.33 (s, 9H). ^{13}C{^{1}H} NMR (75 MHz, $CDCl_3$) *δ* 174.4 (d, *J* = 2.0 Hz), 158.9 (d, *J* = 5.3 Hz), 143.5, 137.9, 137.3, 130.6, 129.3, 128.8, 127.3, 127.2, 120.8 (br), 120.2, 117.0, 36.8, 32.5, 32.5, 19.2. ^{11}B{^{1}H} NMR (96 MHz, $CDCl_3$) *δ* 0.6 (d, *J* = 26.7 Hz). ^{19}F{^{1}H} NMR (282 MHz, $CDCl_3$) *δ* -135.25 (dq, *J* = 84.5, 26.3 Hz), -148.1 (d, *J* = 84.8 Hz). HRMS (ESI$^+$) *m/z* [M+Na]$^+$ calcd for $C_{18}H_{20}{}^{11}B^{19}F_2NNaO$ 338.1504, found 338.1498.

3-(2-(tert-butyl)phenyl)-2,2-difluoro-N,N,4-trimethyl-2H-2λ^4,3λ^4-benzo[e][1,3,2]oxazaborinin-7-amine (9c). Obtained from 190 mg of **14c** as a beige solid (75 mg, 34%) after a chromatography over silica gel (cyclohexane/CH_2Cl_2: 6/4 to 3/7). Mp = 214-218 °C. R_f = 0.66 (cyclohexane/EtOAc: 5/5). ^{1}H NMR (300 MHz, $CDCl_3$) *δ* 7.60 (dd, *J* = 8.1, 1.5 Hz, 1H), 7.47 (d, *J* = 9.2 Hz, 1H), 7.35 (td, *J* = 7.3, 1.7 Hz, 1H), 7.25 (td, *J* = 7.3, 1.6 Hz, 1H), 7.13 (dt, *J* = 7.8, 1.9 Hz, 1H), 6.39 (dd, *J* = 9.2, 2.6 Hz, 1H), 6.32 (d, *J* = 2.6 Hz, 1H), 3.12 (s, 6H), 2.25 (s, 3H), 1.34 (s, 9H). ^{13}C{^{1}H} NMR (75 MHz, $CDCl_3$) *δ* 170.7 (d, *J* = 1.7 Hz), 160.9 (d, *J* = 5.5 Hz), 157.1, 144.4, 138.0, 130.9, 130.3, 128.5, 128.1, 126.9, 107.1, 106.0, 99.7, 40.1, 36.7, 32.55, 32.5, 18.3. ^{11}B{^{1}H} NMR (96 MHz, $CDCl_3$) *δ* 0.6 (d, *J* = 28.9 Hz). ^{19}F{^{1}H} NMR (282 MHz, $CDCl_3$) *δ* -136.6 (dq, *J* = 87.5, 28.4 Hz), -148.6 (dd, *J* = 89.1, 4.3 Hz). HRMS (ESI$^+$) *m/z* [M+Na]$^+$ calcd for $C_{20}H_{25}{}^{11}B^{19}F_2N_2NaO$ 381.1926, found 381.1927.

3-(tert-butyl)-4-(7-(dimethylamino)-2,2-difluoro-4-methyl-2H-2λ^4,3λ^4-benzo[e][1,3,2]oxazaborinin-3-yl)benzonitrile (9d). Obtained from 64 mg of **14d** as a green solid (61 mg, 84%) after a chromatography over silica gel (cyclohexane/CH_2Cl_2: 5/5 to 3/7). Mp = 231-233 °C (dec.). R_f = 0.15 (cyclohexane/CH_2Cl_2 : 4/6). ^{1}H NMR (300 MHz, $CDCl_3$) *δ* 7.89 (d, *J* = 1.8 Hz, 1H), 7.52 (dd, *J* = 8.2, 1.8 Hz, 1H), 7.45 (d, *J* = 9.2 Hz, 1H), 7.26 (d, *J* = 8.2, 1H), 6.39 (dd, *J* = 9.2, 2.5 Hz, 1H), 6.27 (d, *J* = 2.5 Hz, 1H), 3.11 (s, 6H), 2.21 (s, 3H), 1.32 (s, 9H). ^{13}C{^{1}H} NMR (75 MHz, $CDCl_3$) *δ* 170.3 (d, *J* = 1.7 Hz), 161.1 (d, *J* = 5.3 Hz), 157.5, 146.7, 142.4, 134.8, 131.1, 130.2, 130.1, 118.6, 112.5, 106.9, 106.5, 99.6, 40.2, 37.1, 32.3, 32.3, 18.5. ^{11}B{^{1}H} NMR (96 MHz, $CDCl_3$) *δ* 0.5 (d, *J* = 28.4 Hz). ^{19}F{^{1}H} NMR (282 MHz, $CDCl_3$) *δ* -136.1 (dq, *J* = 86.2, 28.0 Hz), -148.1 (dd, *J* = 87.5, 5.2 Hz). HRMS (ESI$^+$) *m/z* [M+Na]$^+$ calcd for $C_{21}H_{24}{}^{11}B^{19}F_2N_3NaO$ 406.1878, found 406.1872.

Computational Details. All calculations were performed with density functional theory (DFT) approach and its time-dependent (TDDFT) variant. A full description of computational details used in these studies is provided in the Supporting Information (SI).

Results and Discussion

SYNTHESIS AND STRUCTURAL CHARACTERIZATION

[2.2]Paracyclophane-based boranils 8

Monosubstituted [2.2]paracyclophanes (PCPs) are an important class of planar chiral scaffolds that are not only widely used in asymmetric synthesis but may also find applications in biological and chirality-related materials sciences.[13] Of particular interest are their emission properties and CPL activity.[14] We thus investigated the preparation of PCP-based boranils **8** by following the general synthetic route depicted in Scheme 1. 4-Amino[2.2]paracyclophane **10**[15] gave imines **12** by a reaction with salicylaldehyde (R = H) or 2-hydroxyacetophenone (R = CH_3) derivatives **11** in presence of titanium ethoxide. A final complexation using $Et_2O{\cdot}BF_3$ in the presence of *N,N*-diisopropylethylamine (DIEA), in refluxing 1,2-dichloroethane (1,2-DCE) for 14 hours yielded the targeted boranils **8**. Note that imine **12a** did not lead to the corresponding boranil **8a** even using stronger conditions; in each case the starting material was recovered. This result could be explained by the steric hindrance of the paracyclophane part and the absence of a stabilizing electron-donating group.

The resulting boranils **8b-d** were fully characterized by ^{1}H, ^{13}C, ^{11}B and ^{19}F NMR, and by mass spectrometry (see Supporting Information, SI). As observed in our previous work on helicene boranils,[10] the ^{11}B NMR signal shows a doublet of doublets (dd) at $\delta \approx 1$ ppm, in agreement with a four-coordinate boron atom, with different coupling constants with the two fluorine atoms (*J* = 22 and 9 Hz at 0.65 ppm for **8c**, for example). The ^{19}F NMR showed doublets of 1:1:1:1 quadruplets (dq) signals for each fluorine that are typical of chiral boranils.

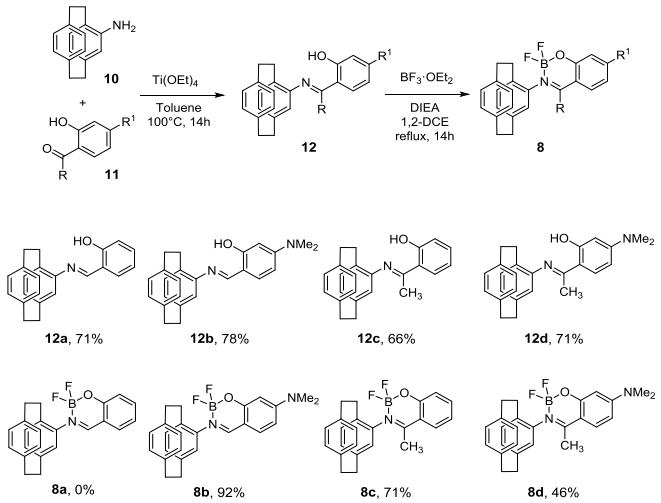

SCHEME 1. Synthesis of [2.2]paracyclophane-based boranils **8**.

Enantiomeric resolution of **8b-d** was then performed using HPLC over chiral stationary phases (see SI). Single crystal of (+)-**8c** was grown by slow diffusion of diisopropylether vapors into CH_2Cl_2 solution, and its structure and stereochemistry was further ascertained by X-ray diffraction crystallography. Indeed, Figure 2 displays the structure of the first eluted enantiomer over a Chiralpak ID© HPLC column, demonstrating a positive optical rotation (OR) and S_p planar chirality ($[\alpha]_\lambda^{25}$ (CH_2Cl_2, *C* 0.1 M) = +372; see SI for HPLC conditions and ORs values). The aforementioned compound (+)-**8c** crystallized in the non-centrosymmetric $P2_12_12_1$ space group and its molecular structure shows a C_1 symmetry. The boranil part displays classical metrics, with O−B and B−N bond-lengths of 1.445 and 1.590 Å, respectively, which are in the range of similar four-coordinate boron(III) derivatives.[Erreur ! Signet non défini.] The PCP unit also shows classical features, with phenyl rings that are almost planar (maximum dihedral angle of 14.92°) and parallel to each other (centroid-centroid distance of 2.978 Å and dihedral angles of CH_2CH_2 bridges as low as -13.49 and 7.49°). Interestingly, the PCP and the boranil parts are linked through an N−C single bond (with a length of 1.456 Å), which displays axial chirality due to a B-N-C_1-C_2 dihedral angle of -76.10°, thus representing the R_a configuration associated with the S_p stereochemistry of the PCP fragment. There is therefore an interesting chiral induction from the paracyclophane part to the axial chirality in the solid state, with the BF_2 group pointing towards the PCP core while the CH_3 faces outward. Close contacts between one fluorine of the BF_2 unit and an aromatic H of a neighboring molecule were also found in the solid.

In order to shed some light on structural and stereochemical preferences for boranils **8** in solution, dispersion-corrected density functional theory (DFT) with continuum solvent model for acetonitrile theoretical calculations were performed using the B3LYP+D3/TZVP basis set; see SI for computational details. The computations involved geometry optimizations for both (R_a,S_p) and (S_a,S_p) epimers of **8a-d** and the corresponding calculations of the energy profile for the full rotation of the PCP unit with respect to the boranil fragment (that is around the N–C_1 axis) in **8b** and **8c** to assess the energetic barriers for the $R_a \leftrightarrow S_a$ atropisomeric transformations. Note that the computations for **8a** were performed only for a completeness of the theoretical studies, as this compound was not obtained experimentally. The representative results obtained for **8c** are shown in Figures 3 and 4; a full set of calculated data can be found in SI.

As illustrated in Figure 3 for **8c**, for each lowest-energy diastereoisomeric (R_a,S_p) and (S_a,S_p) structure of **8** (except (S_a,S_p)-**8a**) two stable and energetically comparable conformers (labelled as **I** and **II**) were found that differ in the position of the boron atom with respect to the plane of the boranil ring, and thus in the relative arrangement of BF_2 and PCP moieties. Namely, with the structure oriented in such a way that the oxygen atom in the boranil fragment faces upward and the PCP unit is placed on the left, in the conformer **I** the boron is positioned 'up' out of the boranil ring (toward the viewer) while in the conformer **II** it is positioned 'down' (away from the viewer). In the case of the boranils **8c** and **8d**, comprising a methyl group on the boranil ring, for both (R_a,S_p) and (S_a,S_p) diastereoisomers, conformers **II** were found (also at the double-hybrid DFT level that is expected to give the most accurate results)[16] to be slightly lower in energy than their corresponding structures **I**, while for **8a** and **8b** that lack such a group no unequivocal energetic preference for **I** or **II** was shown, as for the (R_a,S_p) epimers the former was more stable and for (S_a,S_p) either the latter or the former depending on the compound and (for **8b**) the density functional used in the calculations.

More importantly, however, the calculations revealed that the (S_a,S_p)-**8c** and (S_a,S_p)-**8d** structures demonstrate uniformly higher energy (by ca. 2.9-3.5 kcal mol^{-1}) than their corresponding (R_a,S_p) epimers. Furthermore, as shown for **8c** in Figure 4, the energetic barrier for the $R_a \rightarrow S_a$ conformational chirality transformation was estimated to be rather high, at least 24 kcal mol^{-1}; note that due to similarities between the compounds (the presence of the aforementioned methyl group on the boranil part) the comparably high barrier is also expected for **8d**. Accordingly, all this indicate that the established in the solid state for **8c** induction of chirality may indeed be maintained in solution, and thus both **8c** and **8d** preferentially occur in solution in (R_a,S_p) absolute configuration. On the other hand, for the boranils without the methyl group in their structure, **8a** and **8b**, both (R_a,S_p) and (S_a,S_p) diastereoisomers were computed to be essentially isoenergetic and a noticeable lower (compared to **8c**) energetic barrier for the $R_a \leftrightarrow S_a$ atropisomeric transformations was found for **8b** ($\geq$ 9 kcal mol^{-1}, representative also for **8a**; see SI). Consequently, one may expect these compounds to exist in solution as some mixture of both epimers, although, as established based on computed electronic circular dichroism (ECD) spectra, with the dominance of the (R_a,S_p) configuration in the case of **8b** (*vide infra*).

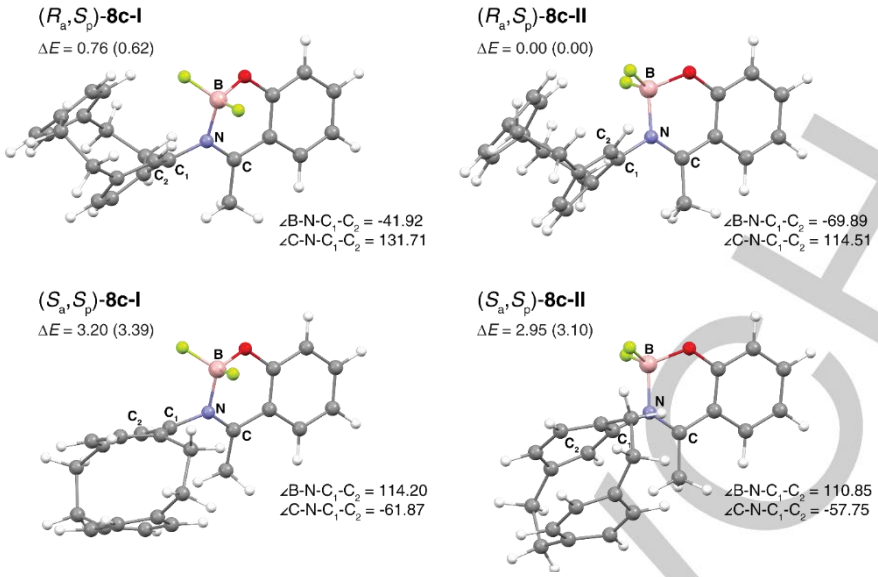

FIGURE 3. Optimized (B3LYP+D3/TZVP with continuum solvent model for acetonitrile) structures of **8c**. Values listed correspond to B-N-C_1-C_2 and C-N-C_1-C_2 dihedral angles (defined on each structure, in degree) and relative energies (based on the B3LYP+D3 and DSD-PBEP86 (in parentheses) calculations, in kcal/mol). Note that (R_a,S_p)-**8c-II** structure corresponds to that found in the X-ray crystal structure of the compound. See SI for the corresponding data for the remaining boranils **8**.

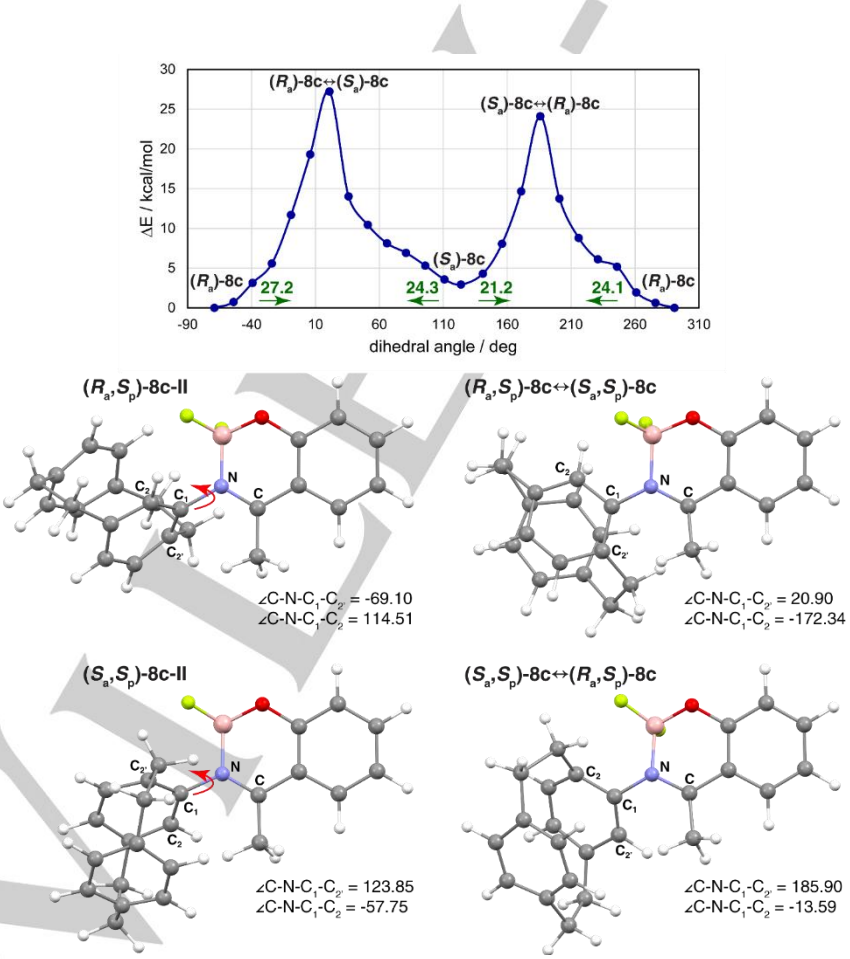

FIGURE 4. Energy profile for the rotation around N–C_1 bond (with the C-N-C_1-$C_{2'}$ dihedral angle as a constraint) in the boranil **8c** (top, to increase legibility, planar chirality descriptor S_p has been omitted in the structures' labels) along with molecular structures corresponding to its characteristic points (bottom). Numbers listed along arrows displayed in the chart are estimated energy barriers (in kcal mol^{-1}) of the transition between two adjacent minima in the direction indicated by the arrow. Based on the B3LYP+D3/TZVP calculations with continuum solvent model for acetonitrile. See SI for the corresponding data for the boranil **8b**.

2-(*t*-Butyl)aniline-based boranils 9

In parallel to paracyclophane-based boranils **8** that exhibit planar chirality, we also explored another family of boron complexes, **9**, comprising *t*-butyl-aniline unit (Scheme 2). The presence of the sterically hindered *t*-butyl group at the *ortho*-position of the aniline (along with the methyl on the boranil unit) should prevent a free rotation around the N–C bond linking the aryl and the boranil fragments, and therefore confer axial chirality to the resulting boranils. In addition to an extremely easy access to **9**, the introduction of the *t*-butyl substituent has also an attractive advantage of hindering packing of difluoroboron complexes in the solid state that should prevent quenching of fluorescence. Following the synthetic pathway for **9** presented in Scheme 2, imines **14** were first synthesized from 2-(*t*-butyl)anilines and salicylaldehyde or 2-hydroxyacetophenones according to similar procedures previously used for compounds **8** and **12**, and then converted to boranils **9** by a treatment with $Et_2O{\cdot}BF_3$ in moderate to good yields.

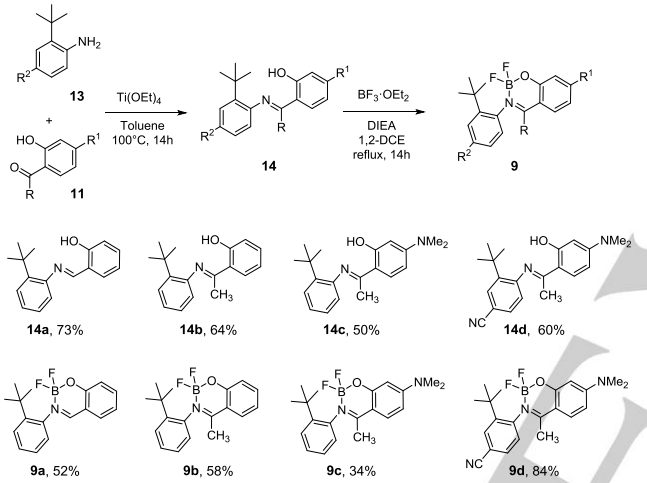

SCHEME 2. Synthesis of 2-(*t*-butyl)aniline-based boranils **9**.

The resulting compounds **9** were fully characterized by NMR and mass spectrometry (see SI). While the ^{1}H and ^{13}C NMR spectra show typical characteristic signals, ^{11}B and ^{19}F NMR deserve special comments.

For example, ^{19}F NMR spectrum of compound **9b** displays two inequivalent coupled signals ($^{2}J_{FF}$ 85 Hz):
- in the -135 ppm region, the ^{19}F signal consists of two overlapping multiplets: 80% dq from ^{11}B-^{19}F at -135.25 ppm ($^{1}J_{BF}$ 26 Hz), and 20% broad signal from ^{10}B-^{19}F at -135.18 ppm.
- in the -148 ppm region, the ^{19}F signal is atypical: two overlapping doublets: 80% d from ^{11}B-^{19}F at -148.13 ppm, and 20% d from ^{10}B-^{19}F at -148.07 ppm. Surprisingly, $^{1}J_{BF}$ is null, and $^{10}B/^{11}B$ isotopic effect is about 30 Hz.

Presence of such a huge isotope effect and null $^{1}J_{BF}$ for -148 ppm fluorine were double-checked using ^{19}F 1D-selective COSY experiments allowing to see selectively ^{10}B- or ^{11}B-coupled fluorine multiplets. Hypothesis of two sets of signals arising from a dimeric compound and / or from an exchange process were ruled out using ^{19}F DOSY and ^{19}F NOESY.

Furthermore, ^{11}B NMR spectrum of **9b** displays a single doublet at 0.6 ppm since only one of the two ^{19}F has a non-zero $^{1}J_{BF}$ coupling constant. Finally, heteronuclear Overhauser effect experiments (2D- or 1D-selective HOESY) reveal that the ^{19}F at -135 ppm is spatially close to the *ortho*-position ^{1}H of the substituted phenyl group, whereas ^{19}F at -148 ppm is spatially close to the *t*-butyl group, hence showing that the rotation around the N-C(aryl) bond is indeed inhibited by the *t*-butyl group at the *ortho*-position.

Single crystals of imine **14b** and boranils (±)-**9a**, (±)-**9b**, (+)- **9c** and (+)-**9d** were grown by slow diffusion of diisopropylether vapors into CH_2Cl_2 solutions, and their structure / stereochemistry were accordingly ascertained by X-ray diffraction crystallography. Interestingly, upon crystallization, boranil **9a** underwent spontaneous resolution and crystallized in the non-centrosymmetric $P2_12_12_1$ space group (see the S_a enantiomer depicted in Figure 2b) while **9b** crystallized in the centrosymmetric $P\text{-}1$ space group. Compounds **9c** and **9d** crystallized in the non-centro-symmetric $P2_12_12_1$ and $P2_1$ space groups, respectively. Figure 2b depicts the structures obtained from the first eluted enantiomers over an (*S*,*S*)-Whelk-O1© HPLC column and having positive OR values for **9c** and **9d** ($[\alpha]_{\lambda}^{25}$ (CH_2Cl_2, *C* 0.1 M) = +380 and +339, respectively; see SI for HPLC conditions and OR values). The molecular structures of **9** show a C_1 symmetry and the boranil metrics are classical. Regarding B–N bond-lengths, they were found of similar orders (1.589 Å for **9b** vs. 1.582 Å for **9d** vs. 1.572 Å for **9c**). Furthermore, the B atom is positioned out of the boranil ring, with the BNO forming a non-zero angle with the NCCCO plane (for example, 29.00° for **9b** and 29.89° for **9c**); see also a description of structures **I** and **II** computed for **8**. This is due to the presence of the bulky *t*-butyl group which forces the BF_2 unit to be placed farther away. Here also, the *t*-butyl-phenyl ring and the boranil parts are linked through an N–C single bond which displays axial chirality in **9c** and **9d** due to B-N-C_1-C_2 dihedral angles of +97.56 and +99.80°, respectively, thus representing the R_a configuration. The combination of *t*-butyl on phenyl and methyl on boranil locks the axial chirality. As a result, an enantiomerization barrier $\Delta G^{\neq}$ of 134.3 kJ mol^{-1} (32.1 kcal mol^{-1}) was experimentally measured in toluene at 110 °C for **9c** (see SI), which corresponds to a half-life time of 25 hours. For **9d**, a slightly decreased enantiomerization barrier $\Delta G^{\neq}$ of 129.2 kJ mol^{-1} (30.9 kcal mol^{-1}) and a smaller half-life time of 5 hours was found under the same conditions, unravelling the strong effect of the *para*-cyano electron-withdrawing group which most probably destabilizes the boranil ring and thus induces enantiomerization upon its opening and re-closure. Along the same hypothesis, compound **9b** which also possesses the *t*-butyl and methyl groups but lacks the *para*-NMe_2 donor group is even less configurationally stable, with an enantiomerization barrier $\Delta G^{\neq}$ of 119.6 kJ mol^{-1} (28.6 kcal mol^{-1}) in toluene at 110 °C and a half-life time as small as 15 minutes at this temperature. In the case of highly labile **9a**, it appeared impossible to separate the two enantiomers by chiral HPLC.

ABSORPTION PROPERTIES (UV-VIS AND ECD)

The UV-vis spectra of **8b-d** and **9b-d**, depicted in Figures 5a and 6a, respectively, were measured between 250 and 450 nm in acetonitrile solution at concentrations *ca.* 10^{-5} M. Compound **8b** displays two bands of low intensity at 270 and 280 nm (ε ~ 4000 M^{-1} cm^{-1}) and an intense band at 395 nm (40000 M^{-1} cm^{-1}), while **8c** demonstrates one intense band at 275 nm (ε ~ 15000 M^{-1} cm^{-1}) and a moderate one at 350 nm (6500 M^{-1} cm^{-1}). Derivative **8d** exhibits a similar UV-vis response as **8b**, *i.e.* two

bands of low intensity at 270 and 280 nm (ε ~ 4000 M^{-1} cm^{-1}) and an intense band at 378 nm (50000 M^{-1} cm^{-1}), in line with the presence of *para*-NMe_2 group in both systems. Regarding the other series, compound **9b** shows an intense band at 270 nm (ε ~ 17000 M^{-1} cm^{-1}) and a moderate one at 345 nm (5000 M^{-1} cm^{-1}), while **9c** displays two bands of low intensity at 270 and 280 nm (ε ~ 4000 M^{-1} cm^{-1}) and an intense band at 375 nm (48000 M^{-1} cm^{-1}). Finally, derivative **9d** exhibits very similar UV-vis response as **9c**, both in shape and magnitude, indicative of the predominant effect of the *para*-NMe_2 group on the excitation characteristics in both systems (*vide infra*).

The ECD spectra of enantiopure samples were then measured (see Figures 5b and 6b, and SI). The different sets of bands observed in UV-vis spectra are ECD-active in both **8** and **9** series. For instance, regarding the first eluted enantiomers of **8** (Figure 5b), (−)- **8b** displays two moderate positive bands at 276 nm ($\Delta\varepsilon$ = +6.7 M^{-1} cm^{-1}) and 300 nm (+7.3 M^{-1} cm^{-1}), and one negative band at 400 nm (−14 M^{-1} cm^{-1}) accompanied by a small negative shoulder at 350 nm. Derivative (+)-**8c** displays a negative band at 263 nm ($\Delta\varepsilon$ = −10.1 M^{-1} cm^{-1}), and two moderate positive ones at 313 nm (+6.3 M^{-1} cm^{-1}), and 355 nm (+7.8 M^{-1} cm^{-1}), while (+)-**8d** shows three negative bands at 267 nm (−3.2 M^{-1} cm^{-1}), 316 nm (−2.3 M^{-1} cm^{-1}) and 376 nm (−9.3 M^{-1} cm^{-1}). For the other series (Figure 6b), (+)-**9b** displays two moderate positive bands at 275 nm ($\Delta\varepsilon$ = +5.7 M^{-1} cm^{-1}) and 348 nm (+4.9 M^{-1} cm^{-1}). Derivative (+)-**9c** demonstrates three positive bands at 275 nm ($\Delta\varepsilon$ = +3.8 M^{-1} cm^{-1}), 320 nm (+3 M^{-1} cm^{-1}) and 370 nm (+11.1 M^{-1} cm^{-1}), while (+)-**9d** shows very similar ECD shape and magnitude as (+)-**9c**.

Finally, Figure 7 presents the absorption dissymmetry factor g_{abs} plots for both series. See also Table 1 for numerical data and a comparison with the g_{lum} values. Interestingly, compounds **8b** and **8d** show similar low-energy g_{abs} values that are one order of magnitude lower than for **8c**. Furthermore, derivatives **9c** and **9d** show similar low-energy values, again one order of magnitude lower than for **9b**. These trends are closely related to the electronic origin and character of the low-energy excitations (π-π* or charge transfer, *vide infra*).

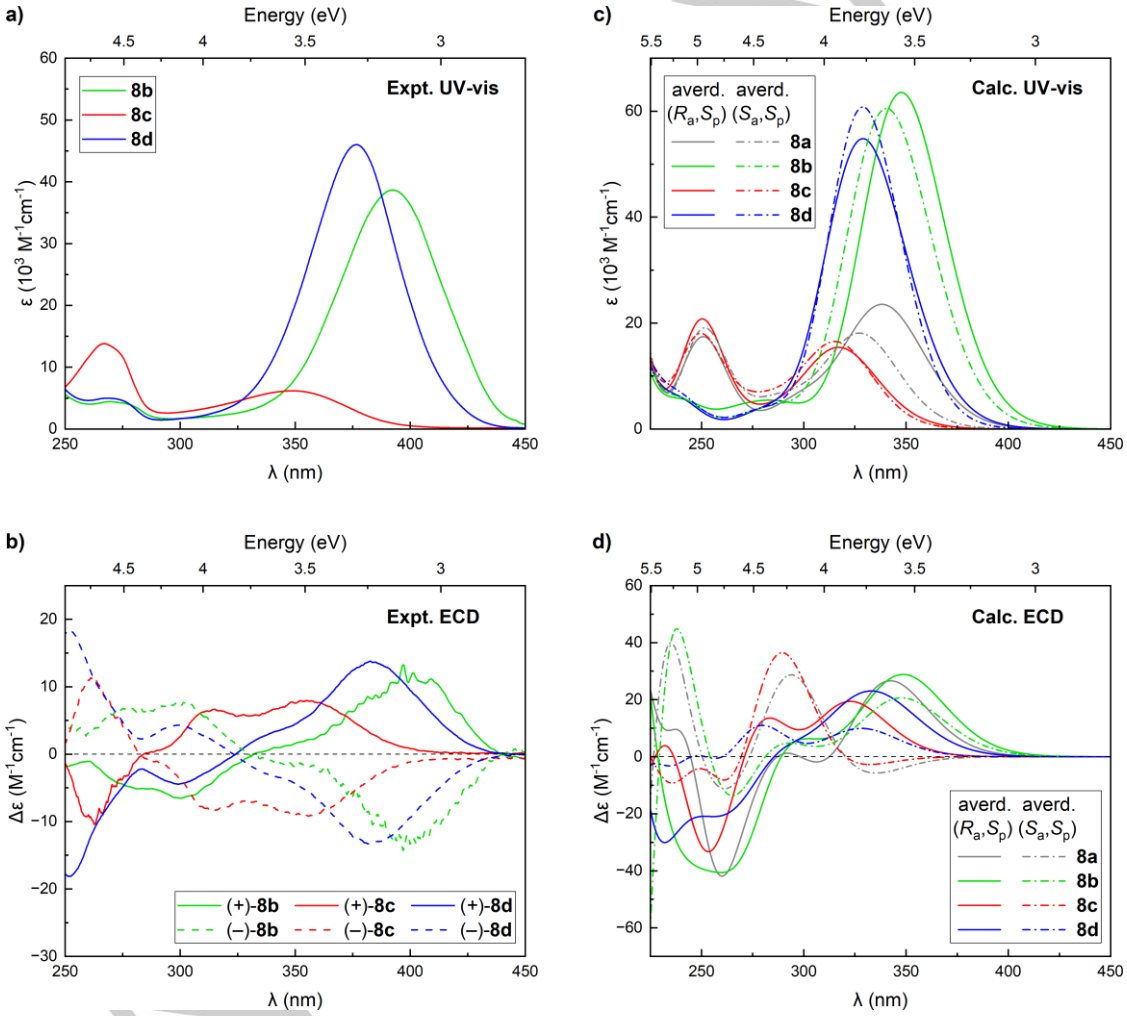

FIGURE 5. Experimental (left, in acetonitrile at r.t. (C ~ 10^{-5} M)) and simulated (right, based on CAM-B3LYP/TZVP calculations with continuum solvent model for acetonitrile, Boltzmann-averaged separately for (R_a,S_p) and (S_a,S_p) diastereoisomers) UV-vis (panels a and c) and ECD (panels b and d) spectra of boranils **8**. See SI for a full set of computed data.

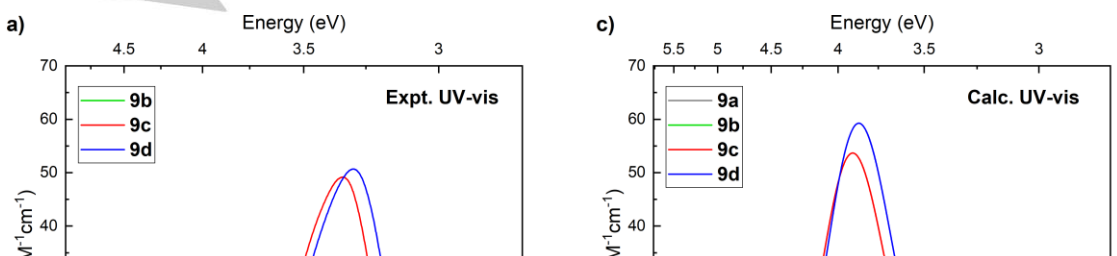

FIGURE 6. Experimental (left, in acetonitrile at r.t. ($C \sim 10^{-5}$ M)) and simulated (right, based on CAM-B3LYP/TZVP calculations with continuum solvent model for acetonitrile) UV-vis (panels a and c) and ECD (panels b and d) spectra of boranils **9**. See SI for a full set of computed data.

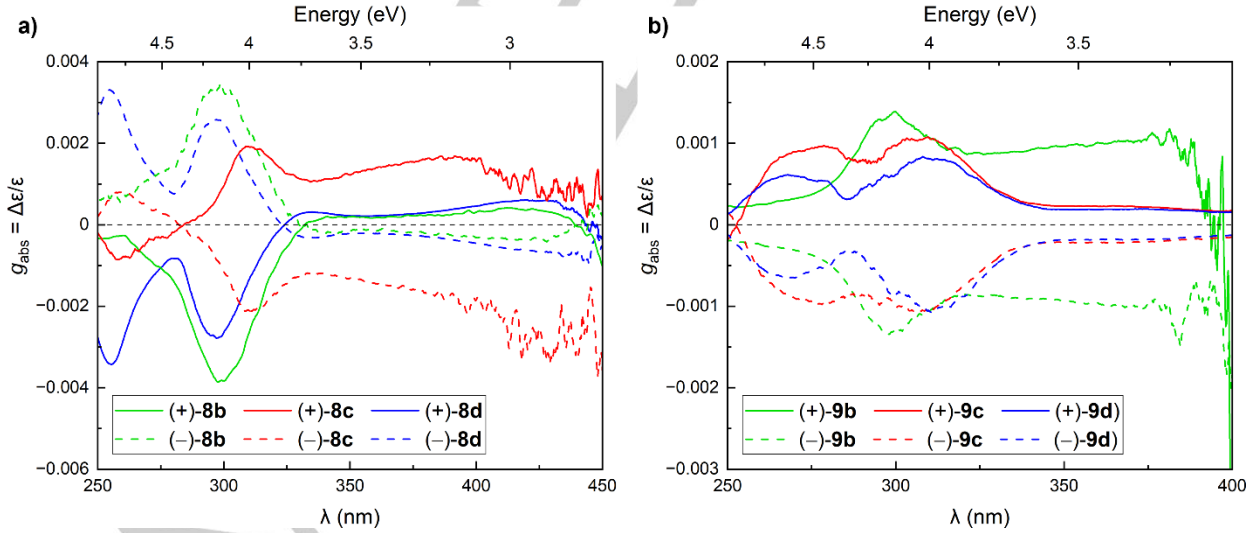

FIGURE 7. Experimental absorption dissymmetry factor g_{abs} plots for a) **8b**-**d** and b) **9b**-**d** series. See also Table 1 for numerical data.

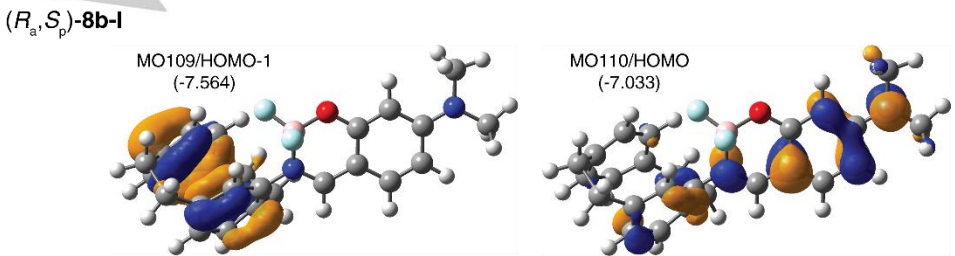

FIGURE 8. Isosurfaces (±0.04 au) of MOs involved in selected electronic transitions of (R_a,S_p)- **8b-I**, (R_a,S_p)- **8c-II**, and (R_a,S_p)- **8d-II**. Values listed in the parentheses are the corresponding orbital energies, in eV. See SI for a full set of computed data.

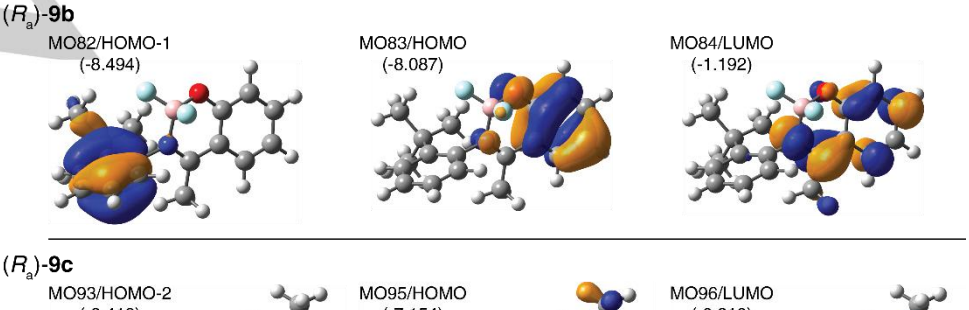

FIGURE 9. Isosurfaces (±0.04 au) of MOs involved in selected electronic transitions of (R_a)-**9b**, (R_a)-**9c**, and (R_a)-**9d**. Values listed in the parentheses are the corresponding orbital energies, in eV. See SI for a full set of computed data.

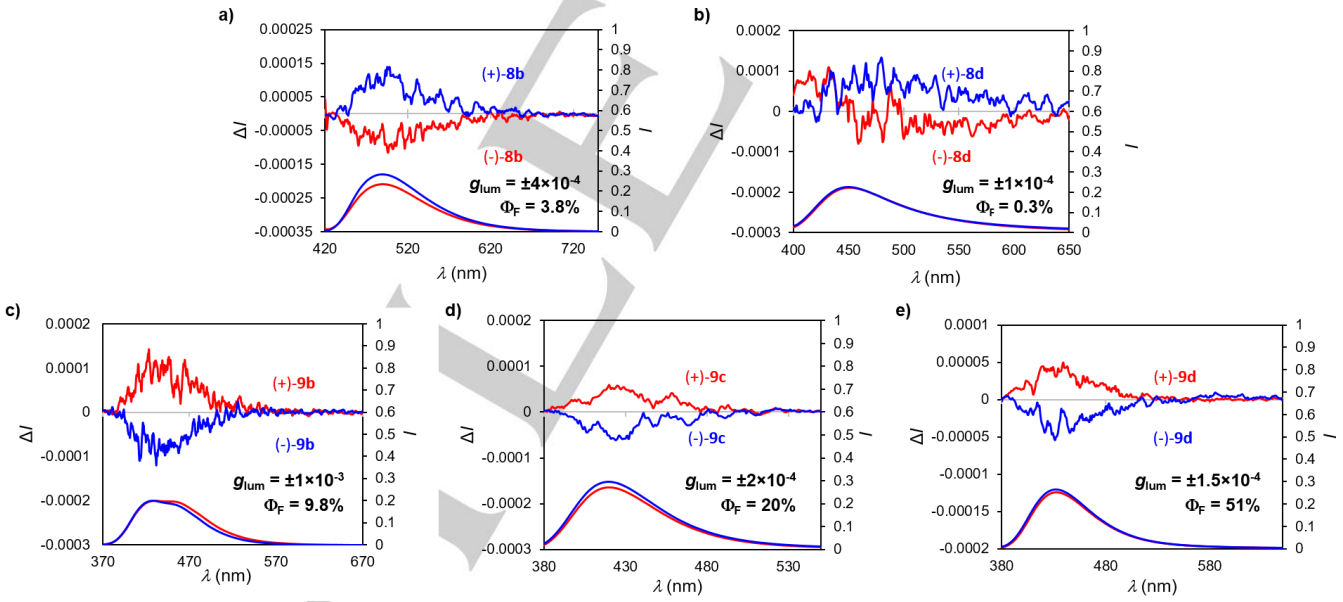

FIGURE 10. Unpolarized and circularly polarized fluorescence spectra (in CH_2Cl_2 at r.t.) of planarly and axially chiral compounds **8b** and **8d** (top), and of axially chiral derivatives **9b**-**d** (bottom).

TABLE 1. Experimental quantum yields, CPL activity (excitation wavelength: 365 nm), and absorption features of (+) enantiomers of boranils **8** and **9**.

System	Φ_F (%)	Solvent	CPL λ_{CPL} (nm)	g_{lum} (at λ_{CPL})	Low-energy absorption λ_{abs} (nm)	ε (M^{-1} cm^{-1}) in CH_3CN[a] (at λ_{abs})	g_{abs} (at λ_{abs})	B_{CPL}
8b	3.8	CH_2Cl_2	490	0.0004	395	40000	0.0003	0.30

8c	0	–	–	–	350	6500	0.0015	0
8d	0.3	CH_2Cl_2	450	0.0001	378	50000	0.0003	0.007
9b	9.8	CH_2Cl_2	425	0.001	345	5000	0.0009	2.45
9c	20	CH_2Cl_2	425	0.0002	375	48000	0.0002	0.96
9d	51	CH_2Cl_2	435	0.00015	380	49000	0.0002	1.87

Φ_F – fluorescence quantum yield (ratio of emitted to absorbed photons). g_{lum} – emission dissymmetry factor. g_{abs} – absorption dissymmetry factor. B_{CPL} – CPL brightness. [a] Molar extinction coefficients were found to be very similar in acetonitrile and in dichloromethane.

Figures 5c and 5d show, respectively, the simulated (using TDDFT-CAM-B3LYP-computed vertical singlet electronic excitations and the corresponding oscillator and rotatory strength values)[17] UV-vis and ECD spectra for **8**, Boltzmann-averaged separately for (R_a,S_p) and (S_a,S_p) diastereoisomers (conformers **I** and **II**, see Figure 3 and SI). As can be seen, overall, all the spectra demonstrate a significant blue-shift compared to experiments, typical for employing in the calculations a density functional with a large fraction of exact exchange.[18] Furthermore, while UV-vis spectral envelopes obtained for the (R_a,S_p) and (S_a,S_p) diastereoisomers are generally quite similar to each other, the ECD spectra significantly differ between these epimers, with those obtained for the (R_a,S_p) structures resembling much bettter – in terms of absolute and / or relative band energies, intensities and the signs – the experimentally measured ones for (+)-**8** enantiomers. This supports further the stereochemical assignment of (+)-**8** as predominantly (R_a,S_p) (*vide supra*). Note, however, that based on the relatively small computed energy barriers for the $R_a \leftrightarrow S_a$ atropisomeric transformations and almost no energy differences between (R_a,S_p) and (S_a,S_p) diastereoisomeric structures for **8b** (and **8a**, modelled only for a completeness of the theoretical studies, as this compound was not obtained experimentally), co-existence of both (R_a,S_p) and (S_a,S_p) epimers in solution may be expected for such system(s) but with a clear dominance of the former as a large population of the latter would produce (unobserved in the experimental data) positive intensity in the higher-energy part of the ECD spectrum for this compound; on the other hand, it should be highlighted that some admixture of (S_a,S_p)-**8b** would decrease the intensity of the low-energy ECD band and thus indeed improve the agreement between the simulated and measured spectra for (+)-**8b** (*vs.* (+)- **8d**).

A satisfactory reproduction of the experimental spectral data for (+)-**8** by the calculations for their respective (R_a,S_p) epimers enabled assignment of particular bands *via* analysis of underlying dominant excitations in terms of MO-to-MO contributions. It is worth recollecting that the presented simulated spectra of (R_a,S_p)-**8** represent in each case a Boltzmann-averaged spectrum obtained for two considered conformers **I** and **II**, see Figure 3 and SI. As presented in SI, such two corresponding structures demonstrate overall similar spectral envelopes although the ones computed for **II** are always blue-shifted and generally less intense as compared to those for **I** (the same is also true for (S_a,S_p)-**8**, see Figure S2.7). The corresponding MOs for the conformers look very alike, and, although MO-pair contributions for particular excitations are sometimes different, general assignment of the particular bands in both cases is the same. The aforementioned energetic shift of the spectra for the structures **II** *vs.* **I** correlates with the observed in the former conformers *vs.* the latter noticeable energetic destabilization of the lowest unoccupied MOs, and a consequent increase in gap(s) between high-lying occupied orbitals and LUMO predominantly involved in the dominant excitations in the considered spectral range. The spectral analysis demonstrated further that the low-energy (observed experimentally at wavelengths longer than *ca.* 325 nm) UV-vis and ECD intensities for the compounds comprising *para*-NMe_2 group grafted on the boranil fragment, **8b** and **8d**, originate from the lowest-energy excitation (no. 1) assigned as almost pure π-π^* transition within boranil-based moiety (and to a much smaller degree within PCP fragment). The transition involves the frontier MOs, HOMO and LUMO, both delocalized over π-conjugated electron system of the boranil-NMe_2 and partially spread also over the connected phenyl ring of PCP (see Figure 8 and SI). The red-shift of this band visible for **8b** *vs.* **8d** may be rationalized by an increase in the HOMO-LUMO gap observed for the latter system (**8d**), occurring as a result of energetic destabilization of the LUMO level, likely due to the effect of the *ortho*-Me group. For **8c** (and **8a**), missing the amine group in the molecular structure, the low-energy part of the UV-vis and ECD spectra observed in the experiments between *ca.* 275 and 400 nm, *i.e.* at much blue-shifted wavelengths compared to **8b** and **8d**, stems from three excitations of sizeable oscillator (*f*) and / or rotatory (*R*) strengths (with alternating sign pattern in the case of *R*, explaining appearence of two bands in this spectral region). These excitations involve boranil-centered LUMO and high-energy occupied MOs localized mainly on either the PCP unit (HOMO, HOMO-1, HOMO-2) or the boranil (HOMO-3), and they are thus attributed to a mix of PCP→boranil charge-transfer (CT) and π-π^* within the boranil transitions. The striking difference between the spectral envelopes for **8c** and for **8b**,**d** can be therefore easily traced back to the lack of the electron-donating *para*-NMe_2 group. Without this group, the π-electron system of the boranil moiety is less extended in **8c** (as compared to **8b**,**d**), and accordingly it demonstrates a decreased (more stabilizing) orbital energy of its corresponding occupied MOs. As a result, HOMO for **8c** is PCP-centered and the aforementioned low-energy CT states are induced. As far as higher-energy intensity, observed in the UV-vis and ECD for **8b**-**d** at wavelengths shorter than *ca.* 275 (for **8c**) and 300 (for **8b**,**d**) nm, is concerned, the analyses revealed that it originates from a mixture of PCP→boranil and boranil→PCP CT and boranil- and PCP-centered π-π^* transitions. Notably, a clear UV-vis band observed in this spectral region for **8c** comes from the excitations of the mix boranil-centered π-π^* and PCP→boranil CT character.

The TDDFT-CAM-B3LYP-simulated UV-vis and ECD spectra of the boranils **9a**-**d** (note that the calculations for **9a** were performed only for a completeness of the theoretical studies, as for this compound no spectral measurements were conducted), presented respectively in Figures 6c and 6d, also demonstrate the aforementioned blue-shift (*vs.* experiments) linked with the large amount of exact exchange in the density functional used in the calculations, but again, generally agree well with the experimentally measured responses, in terms of the reproduction of relative bands positions, intensities and the signs. Regarding the latter, the perfect correspondence between ECD spectra experimentally measured for (+)-**9** enantiomers with those computed for (R_a)-**9** structures, ultimately confirms their

stereochemical assignment. The most striking discrepancy between computations and experiments, apart from a visible deficiency in a description of a spectral substructure (somewhat more noticeable as compared to **8**) due to neglecting of vibronic effects in the former, is observed for the position of the higher-energy ECD band for (R_a)-**9b** that in the simulated spectra appears visibly red-shifted compared to (R_a)-**9c**,**d**, while experimentally all three compounds demonstrate the same energetic position of this band. Analysis of MO-pair contributions to dominant excitations for **9a**-**d** showed that the low-energy intensity of the UV-vis and ECD spectra for these compounds observed experimentally at wavelengths longer than *ca.* 300 nm originates predominantly from the lowest-energy excitation (no. 1) corresponding to almost pure HOMO-to-LUMO π-π* transition within boranil-based fragment; for **9c**,**d** excitation no. 2 of similar assignment although involving HOMO-1 and LUMO was also found to be responsible for the broad ECD band at this spectral region. Importantly, as can be seen in Figure 9 and SI, in the case of **9c**,**d** the aforementioned orbitals span over the whole boranil fragment including nitrogen atom of the *para*-NMe_2 group, thus showing more extended π-electron system in this unit as compared to **9a**,**b** (as it was notice for **8b**,**d** *vs.* **8c** (and **8a**)). This may explain a red-shift of the corresponding band and an increase in its intensity visible in experimental and computed spectra for **9c**,**d** *vs.* **9b**. Moreover, inspection of the orbital energies revealed that a slight red-shift of the intense lowest-energy peak observed in spectra of **9d** *vs.* **9c** correlates with a decreased HOMO-LUMO gap for the former system that appears to originate from a stabilization of the LUMO level likely due to the presence of the *para*-cyano group in the system. Regarding the higher-energy intensity observed in the UV-vis and ECD for **9b**-**d** at wavelengths shorter than *ca.* 300 nm, the computations showed that for **9a**-**c** it is assigned to admixed *t*-butyl-phenyl→boranil CT and boranil-centered π-π* transitions, whereas for **9d** it is attributed predominantly to combined boranil→*t*-butyl-phenyl CT and *t*-butyl-phenyl-centered π-π* transitions, both involving the cyano group, and some *t*-butyl-phenyl→boranil CT and π-π* within boranil fragment excitations appearing at higher energies. The change in the character of the dominant excitations for the latter system (**9d**) can be again traced back to the presence of the *para*-cyano group that has a stabilizing effect on the *t*-butyl-phenyl-localized unoccupied MOs (see Figure 9 and SI).

EMISSION PROPERTIES (UNPOLARIZED AND CIRCULARLY POLARIZED FLUORESCENCE)

The luminescence properties of compounds **8b**-**d** and **9b**-**d** were examined in CH_2Cl_2 at room temperature (r.t., 298 K); see Figure 10 and Table 1. While **8c** displayed too low emission to be measured, compounds **8b**,**d** exhibited fluorescence signals centered at 490 and 450 nm, respectively (see Figures 10a,b), with moderate to low quantum yields. The series **9b**-**d** displayed much stronger fluorescence with quantum yields ranging from 9.8 to 51% (Figures 10c,d,e).

Interestingly, chiral boranils are known to exhibit circularly polarized fluorescence, which makes them appealing for incorporation into OLEDs as circularly polarized electroluminescent materials.[10,11] Satisfyingly, the enantiomers **8b**,**d** and **9b**-**d** revealed almost mirror-image CPL activity (Figure 10). Regarding the dissymmetry factors, which reflect the percentage of circularly polarized emitted light ($g_{lum} = 2(I_L - I_R)/(I_L + I_R)$), the values ranged from 1×10^{-4} to 1×10^{-3}, with positive signals for the (+) enantiomers (and *vice versa*) and with the highest value being found for **9b** (see Table 1). Interestingly, the g_{lum} values show similar magnitudes as the g_{abs} ones. Overall, although moderate, these results show that circularly polarized fluorescent emitters can be obtained by introducing boranil units in very simple building blocks. As proposed by Zinna and coworkers,[19] one may consider the CPL brightness, defined as $B_{CPL} = \varepsilon \times \Phi \times g_{lum} / 2$ (where ε is taken at the excitation wavelength). By this way, we take into account the overall process through absorption, quantum yield and dissymmetry factors efficiencies. Values between 0.007 and 2.45 are obtained, appearing quite small compared to other classes of PCP systems (that can reach 300) and other boron derivatives such as BODIPY (up to 159).[19] This is most probably due to the fact that the boranil units are not fused to the chiral core but rather placed at its periphery.

Conclusions

In summary, we have prepared two new series of boranil derivatives, displaying planar and / or axial chirality. Their structural, photophysical and chiroptical properties have been studied in detail. Notably, X-ray structure crystallography and theoretical analysis revealed the presence (and stability) of both planar and axial chiralities together with co-existence of different conformers for the **8a**-**d** boranil series. These compounds display moderate ECD responses, but low fluorescence quantum yields and CPL activities. In comparison, boranils **9a**-**d** exhibiting axial chirality only, reveal similarly moderate ECD fingerprints but higher fluorescence quantum yields and stronger CPL signals (higher g_{lum} values up to 1×10^{-3}), resulting in stronger CPL brightness. This work highlights the fact that sophisticated chiral architectures are not necessary to achieve typical g_{lum} and brightness values in chiral organic luminophores. Nevertheless, the overall performance of the systems reported herein remains modest compared to other recently described planarly chiral boranils or other classes of boron derivatives.

Supporting Information Summary

Detailed information about the spectral characterizations such as ^{1}H, ^{13}C, ^{19}F and ^{11}B NMR along with HRMS spectra of all synthesized products; HPLC conditions; photophysical and chiroptical studies, and X-ray diffraction data for compounds **8**, **9** and **14b**; description of computational details along with additional calculated data.

Acknowledgements

We acknowledge the Centre National de la Recherche Scientifique (CNRS) and the University of Rennes. The computational part of this work was supported by PL-Grid Infrastructure and the ACC Cyfronet AGH in Krakow, Poland. The European Commission Research Executive Agency (Grant Agreement number: 859752 – HEL4CHIROLED – H2020-MSCA-ITN-2019) is thanked for financial support.

Conflict of Interest

The authors declare no conflict of interest.

REFERENCES AND NOTES

1. For recent book and reviews, see: a) Mori T (Ed), Circularly Polarized Luminescence Of Isolated Small Organic Molecules, Springer, **2020**; b) Li X, Xie Y, Li Z. The Progress of Circularly Polarized Luminescence in Chiral Purely Organic Materials. *Adv Phot Res* **2021**;2:2000136; c) Li C, Duan P. Recent Advances Of Circularly Polarized Luminescence In Photon Upconversion Systems. *Chem Lett* **2021**;50:546-552; d) Meskers SC. Circular Polarization Of Luminescence As A Tool To Study Molecular Dynamical Processes. *ChemPhotoChem* **2022**;6:e202100154; e) Zhang D-W, Li M, Chen C-F. Recent Advances In Circularly Polarized Electroluminescence Based On Organic Light-Emitting Diodes. *Chem. Soc. Rev.* **2020**;49:1331-1343; f) Nitti A, Pasini D. Aggregation-Induced Circularly Polarized Luminescence: Chiral Organic Materials For Emerging Optical Technologies Advanced Materials. *Adv Mat* **2020**;*32*:1908021; g) Zhao T, Han J, Duan P, Liu M. New Perspectives To Trigger And Modulate Circularly Polarized Luminescence Of Complex And Aggregated Systems: Energy Transfer, Photon Upconversion, Charge Transfer, And Organic Radical. *Acc Chem Res* **2020**;53:1279-1292.

2. Mellerup SK, Wang S. Boron-Based Stimuli Responsive Materials. *Chem Soc Rev* **2019**;48:3537-3549.

3. Treibs A, Kreuzer F-H. Difluorboryl-Komplexe von Di- Und Tripyrrylmethenen. *Liebigs Ann Chem* **1968**;718:208-223.

4. For recent reviews, see: a) Poddar M, Misra R. Recent Advances Of BODIPY Based Derivatives For Optoelectronic Applications. *Coord Chem Rev* **2020**;421:213462; b) Squeo BM, Gregoriou VG, Avgeropoulos A, Baysec S, Allard S, Scherf U, Chochos CL. BODIPY-Based Polymeric Dyes As Emerging Horizon Materials For Biological Sensing And Organic Electronic Applications. *Prog Polym Sci* **2017**;71:26-52; c) Squeo BM, Pasini M. BODIPY Platform: A Tunable Tool For Green To NIR Oleds. *Supramol Chem* **2020**;32:56-70; d) Lu P, Chung K-Y, Stafford A, Kiker M, Kafle K, Page ZA. Boron Dipyrromethene (BODIPY) In Polymer Chemistry. *Polym Chem* **2021**;12:327-348; e) Li F-Z, Yin J-F, Kuang G-C, BODIPY-Based Supramolecules: Construction, Properties And Functions. *Coord Chem Rev* **2021**;448:214157.

5. Li D, Zhang H, Wang Y. Four-Coordinate Organoboron Compounds For Organic Light-Emitting Diodes (Oleds). *Chem Soc Rev* **2013**;42:8416-8433.

6. Massue J, Jacquemin D, Ulrich G. Boranils: Versatile Multifunctional Organic Fluorophores For Innovative Applications. *Organics* **2021**;2:365-375.

7. Zhou Y, Kim JW, Kim MJ, Son W-J, Han SJ, Kim HN, Han S, Kim Y, Lee C, Kim S-J, Kim DH, Kim J-J, Yoon J. Novel Bi-Nuclear Boron Complex With Pyrene Ligand: Red-Light Emitting As Well As Electron Transporting Material In Organic Light-Emitting Diodes. *Org Lett* **2010**;12:1272-1275.

8. Vaz PA, Rocha J, Silva AM, Guieu S. Aggregation-Induced Emission Enhancement Of Chiral Boranils. *New J Chem* **2018**;42:18166-18171.

9. Jiang Z, Wang X, Ma J, Liu Z. Aggregation-Amplified Circularly Polarized Luminescence From Axial Chiral Boron Difluoride Complexes. *Sci China Chem* **2019**:62;355-362.

10. Macé A, Hamrouni K, Gauthier ES, Jean M, Vanthuyne N, Frédéric L, Pieters G, Caytan E, Roisnel T, Aloui F, Srebro-Hooper M, Carboni B, Berrée F, Crassous J. Circularly Polarized Fluorescent Helicene-Boranils: Synthesis, Photophysical And Chiroptical Properties. *Chem Eur J* **2021**;27:7959-7967.

11. a) Chen C-H, Zheng W-H. Planar Chiral Boron Difluoride Complexes Showing Circularly Polarized Luminescence. *Org Chem Front* **2021**;8:6622-6627; b) Li K, Ji H, Yang Z, Duan W, Ma Y, Liu H, Wang H, Gong S. 3D Boranil Complexes with Aggregation-Amplified Circularly Polarized Luminescence. *J Org Chem* **2021**;86:16707-16715. For other types of CPL-active B−N heteroarenes based on [2.2]paracyclophane see: c) Chen C-H, Zheng W-H. Planar Chiral B−N Heteroarenes Based On [2.2]Paracyclophane As Circularly Polarized Luminescence Emitters. *Org Lett* **2021**;23:5554−5558. For chiral boron-ketoiminate systems see: d) Lozada IB, Ortiz RJ, Braun JD, Williams JAG, Herbert DE. Donor−Acceptor Boron-Ketoiminate Complexes With Pendent N- Heterocyclic Arms: Switched-on Luminescence through N- Heterocycle Methylation. *J Org Chem* **2022**;87:184-196.

12. García-Valle FM, Estivill R, Gallegos C, Cuenca T, Mosquera MEG,Tabernero V, Cano J. Metal And Ligand-Substituent Effects In The Immortal Polymerization Of *Rac*-Lactide With Li, Na, And K Phenoxo-imine Complexes. *Organometallics* **2015**;34:477−487.

13. a) Hassan Z, Spuling E, Knoll DM, Bräse S. Regioselective Functionalization Of [2.2]Paracyclophanes: Recent Synthetic Progress And Perspectives. *Angew Chem Int Ed* **2020**;59:2156-2170; b) Felder S, Wu S, Brom J, Micouin L, Benedetti E. Enantiopure Planar Chiral [2.2]Paracyclophanes: Synthesis And Applications In Asymmetric Organocatalysis. *Chirality* **2021**;33:506-527.

14. Sugiura K-I. [2.2]Paracyclophane-Based Chiral Platforms For Circularly Polarized Luminescence Fluorophores And Their Chiroptical Properties: Past And Future. *Front Chem* **2020**;8:700.

15. a) Braun C, Spuling E, Heine NB, Cakici M, Nieger M, Bräse S. Efficient And Modular Synthesis Of Isomeric Mono- And Bis-Pyridyl-[2.2]Paracyclophanes By Palladium Catalyzed Cross-Coupling Reactions. *Adv Synth Catal* **2016**;358:1664-1670; b) Jayasundera KP, Kusmus DNM, Deuilhé L, Etheridge L, Farrow Z, Lun DJ, Kaura G, Rowlands GJ. The Synthesis Of Substituted Amino[2.2]-Paracyclophanes. *Org Biomol Chem* **2016**;14:10848-10860.

16. Goerigk L, Mehta N. A Trip To The Density Functional Theory Zoo: Warnings And Recommendations For The User. *Aust J Chem* **2019**;72:563-573.

17. a) Srebro-Hooper M, Autschbach, J. Calculating Natural Optical Activity Of Molecules From First Principles. *Annu Rev Phys Chem* **2017**;68:399-420; b) Autschbach J. Computing Chiroptical Properties With First-Principles Theoretical Methods: Background And Illustrative Examples. *Chirality* **2009**;21:E116-E152.

18. a) Jacquemin D, Perpète EA, Scuseria GE, Ciofini I, Adamo C. TD-DFT Performance For The Visible Absorption Spectra Of Organic Dyes: Conventional Versus Long-Range Hybrids. *J Chem Theory Comput* **2008**;4:123-135; b) Goerigk L, Casanova-Paéz M. The Trip To The Density Functional Theory Zoo Continues: Making A Case For Time-Dependent Double Hybrids For Excited-State Problems. *Aust J Chem* **2021**;74:3-15.

19. Arrico L, Di Bari L, Zinna F, Quantifying The Overall Efficiency Of Circularly Polarized Emitters. *Chem Eur J* **2021**;27:2920-2934.

Graphical Abstract